AIChE

Continuous Precipitation of L-Asparagine Monohydrate in a Micromixer: Estimation of Nucleation and Growth Kinetics

Christian Lindenberg and Marco Mazzotti
Institute of Process Engineering, ETH Zurich, CH-8092 Zurich, Switzerland

DOI 10.1002/aic.12326
Published online July 20, 2010 in Wiley Online Library (wileyonlinelibrary.com).

An experimental setup based on a static micromixer is used to determine nucleation and growth kinetics of L-asparagine monohydrate precipitated via antisolvent addition. Mixing in static micromixers was characterized previously using competitive-parallel reactions and computational fluid dynamics (Lindenberg et al., Chem Eng Sci. *2008;63:4135–4149). In this work, the mixer setup is used to determine nucleation and growth kinetics of L-asparagine at high supersaturations, i.e., true kinetics which are not affected by transport limitations. The method is based on measuring the particle size distribution obtained at different residence times. A population balance equation model of the process is used for the design of a continuous precipitation process. Finally, an analysis of the characteristic time scales of nucleation, growth, and mixing shows that, under the conditions in this study, mixing is much faster than precipitation and that the two processes can be decoupled.* © 2010 American Institute of Chemical Engineers *AIChE J,* 57: 942–950, 2011

Keywords: L-asparagine monohydrate, nucleation, growth, continuous precipitation, Y-mixer

Introduction

The attainment of fast mixing is a requirement to avoid transport limitations in processes with fast kinetics such as precipitation at high supersaturations. Precipitation is often conducted under these conditions to produce small particles with a narrow particle size distribution (PSD). Stahl and Rasmuson[1] have developed a model combining meso- and micromixing with the population balance equation (PBE) to describe single-feed semibatch reactive crystallization of benzoic acid. It was shown that feed position, feed pipe diameter, feeding time, feed concentration, stirring rate, and reactor volume all had an effect on the final particle size. Similar results were found in several other studies,[2–5] thus suggesting that reactive or antisolvent precipitations should rather be carried out in a different kind of setup, e.g., a static mixer with high mixing performance.

Confined impinging jet (CIJ), T- and Y-mixers are often applied to carry out precipitation processes at high supersaturations.[6] Peukert and coworkers[7] have investigated the effect of mixing on nanosized particles precipitated in a T-mixer. They could clearly observe a decrease in particle size with increasing power input. Their model included direct numerical simulation of the flow, Lagrangian particle tracking, and population balance modeling incorporating nucleation, growth, and agglomeration kinetics. Braatz and coworkers[8] have simulated the antisolvent precipitation of Lovastatin using a combined computational fluid dynamics (CFD)–PBE model of a CIJ reactor and could reproduce the same trends, i.e., decreasing particle size with increasing Reynolds number, as obtained experimentally by Mahajan and Kirwan.[9] In the last work, it was found that if the characteristic time

Correspondence concerning this article should be addressed to M. Mazzotti at marco.mazzotti@ipe.mavt.ethz.ch.

scale for mixing is much smaller than the induction time, in this case about three times smaller, the precipitation process is not affected by the mixing conditions. When compared with T-, Y- or vortex mixers, the use of CIJ reactors is less beneficial in antisolvent precipitation because the values of the momentum of the two streams should be same for the mixer to be effective,[10] and this is not always possible in antisolvent precipitation.

CFD in combination with PBE models can be used to predict the influence of mixing on the PSD and thus they can be used for the design, optimization, and scale-up of precipitation processes. The main problem to the routine use of CFD–PBE models is the identification of true kinetics, i.e., kinetics which are not affected by transport limitations. Static mixers have been used previously to determine nucleation and growth kinetics in antisolvent[11,12] or reactive precipitation processes.[13,14] Kirwan and Mahajan[11] determined independently nucleation and growth rates of L-asparagine monohydrate using a grid mixer and based on the measured PSDs at different residence times. Other studies use the measured PSDs at the outlet of the mixer together with a population balance model and a nonlinear optimization algorithm to estimate simultaneously the parameters in the nucleation and growth rate expressions.[13,14]

In this work, different methods for the determination of nucleation and growth kinetics in static mixers are compared for the antisolvent precipitation of L-asparagine monohydrate. First, the nucleation and growth rates are determined independently by measuring the PSD at different time intervals, whereas the nucleation rate is calculated from the change of the particle concentration over time and the growth rate is determined based on the evolution of the average particle size. Second, the nucleation and growth kinetics are estimated simultaneously based on the experimental data by combination with a population balance model and an integral parameter estimation technique. These methods can only be applied if the time scales for mixing are much smaller than those for precipitation. Therefore, thirdly, a time scale analysis is carried out comparing the time scales for nucleation and growth of L-asparagine monohydrate with the mixing time scales determined earlier.[6,15] Decoupling precipitation and mixing can be achieved by properly choosing the operating conditions, e.g., by increasing the flow rate or decreasing the supersaturation. Regarding the application in industry, this decoupling is beneficial because small changes in the flow rate or scaling of the reactor walls will not have an influence on the particle size in a continuous precipitation process. Moreover, the processes can be designed without using a CFD–PBE model, thus making the process design easier, as shown in the results section.

Experimental Section

Materials and methods

The solute and the antisolvent stream are mixed in a Y-mixer using a custom-made setup, consisting of two pressure tanks, which allow for pulsation-free flows and high pressure drops. A schematic of the experimental setup and the Y-mixer is given in Figure 1. The tanks are pressurized with nitrogen. The flow rate, pressure, and temperature can be measured in both streams. The mixing efficiency of the Y-mixer has been characterized previously using competitive-parallel chemical reactions and CFD.[6]

L-Asparagine monohydrate was precipitated at 25°C from an aqueous solution by mixing it with 2-propanol as antisolvent. L-Asparagine monohydrate (>99%, Sigma–Aldrich, Buchs, Switzerland), 2-propanol (>99.8%, Sigma–Aldrich, Buchs, Switzerland), and deionized water were used in all experiments. The supersaturation was varied by changing the flow rate ratio of the two streams. The initial concentration of L-asparagine monohydrate in the aqueous solute stream was kept constant at 15 g/kg in all experiments. The supersaturation is defined as follows:

$$S = \frac{c}{c^*(w)}, \tag{1}$$

with c and c^* being the concentration and solubility of L-asparagine monohydrate, respectively, and w being the antisolvent weight fraction. The measured solubility of L-asparagine monohydrate in water–2-propanol solutions is given in the following section. The flow rate ratio was changed from 1:1 to 1:20 (aqueous solute solution:antisolvent) yielding initial supersaturation levels from about 4–170.

The pressure drop across the mixer was kept constant at 10 bar in all experiments, which corresponds to a mixing time of about 2 ms.[6]

L-Asparagine can precipitate as monohydrate or as anhydrous solid. The two forms can be distinguished through their Raman spectra which exhibit clear differences. In all experiments, only the monohydrate of L-asparagine was precipitated. The Raman spectra were measured using a RA 400 Raman spectrometer from Mettler-Toledo (Greifensee, Switzerland).

PSDs were measured using a Multisizer 3 from Beckman Coulter (Nyon, Switzerland).

Solubility measurement

The solubility of L-asparagine monohydrate in aqueous solution at 25°C was measured in the range of 50–90 wt % 2-propanol by high performance liquid chromatography (HPLC) analysis of saturated solutions. A HPLC system from Waters (Waters GmbH, Eschborn, Germany) with a 125-mm GROM-SIL 100 ODS-2 column (Alltech Grom GmbH, Rottenburg-Hailfingen, Germany), a variable wavelength UV detector, and an aqueous mobile phase containing 0.1 wt % NaH_2PO_4 as a buffer were used in all experiments. For each solvent composition, at least three equilibrated samples were prepared. Each sample was injected three times into the HPLC system. The measured solubility and the corresponding standard deviation are given in Table 1.

The measured solubilities are also plotted in Figure 2 together with data from literature.[16] The differences between the experimental and the literature values are marginal for a 50 wt % solution but are quite significant at higher 2-propanol concentrations. It can be observed that the experimental data of this study are always below the literature data. We have decided to use our data in the following.

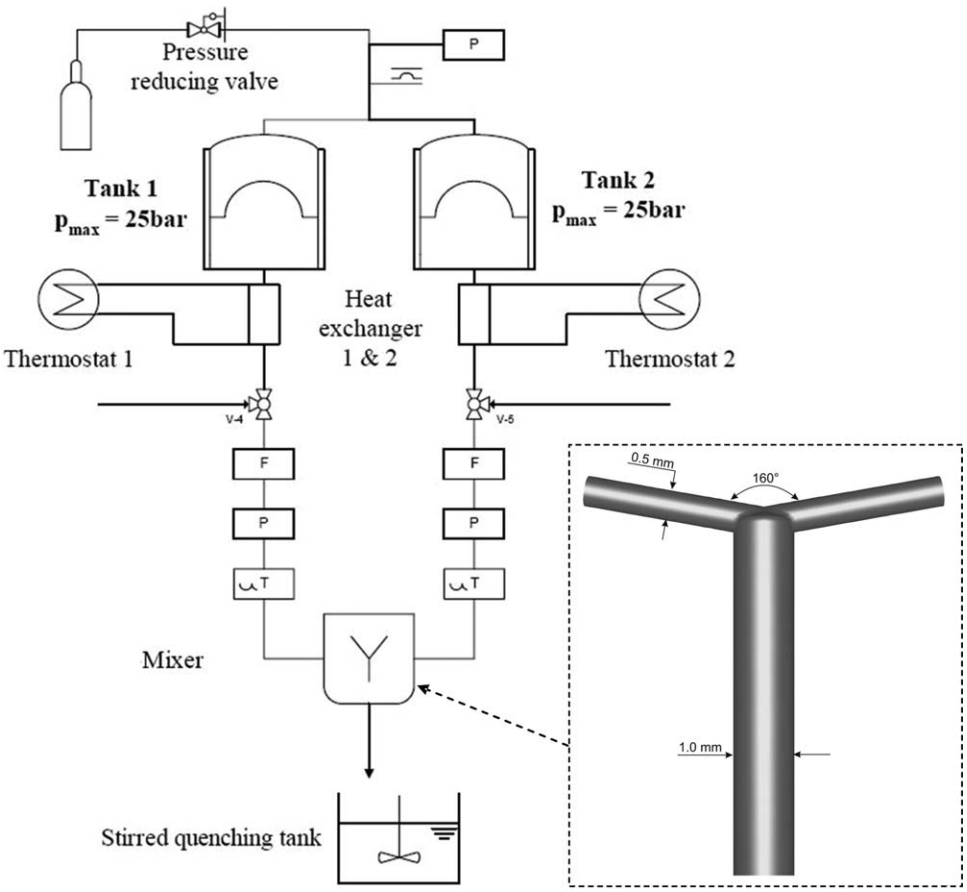

Figure 1. Experimental setup and Y-mixer geometry.

For further analysis, the polynomial given by Eq. 2 is used to describe the solubility as a function of antisolvent concentration. Note that the polynomial is only valid at 25°C and in the range from 0 to 90 wt % 2-propanol and should not be extrapolated:

$$\log_{10}(c^*) = -6.22w^3 + 5.22w^2 - 3.30w + 1.46, \qquad (2)$$

where c^* is given in g L-asparagine monohydrate per kg of solvent and w is the solute-free weight fraction of 2-propanol.

Results and Discussion

Measurement of the precipitation kinetics

Nucleation Kinetics. The nucleation rate is determined by measuring the PSD at different time intervals.[11] Assuming agglomeration and breakage are negligible, the nucleation rate can be calculated from the change of the number of crystals over time as:

Table 1. Solubility of L-Asparagine Monohydrate at 25°C in Water–Isopropanol Solutions

w (g/g)	c^* (g/kg solvent)	Standard Deviation (%)
0.5	2.18×10^{0}	0.65
0.6	9.77×10^{-1}	1.5
0.7	4.28×10^{-1}	1.7
0.8	9.43×10^{-2}	1.5
0.9	1.51×10^{-2}	3.8

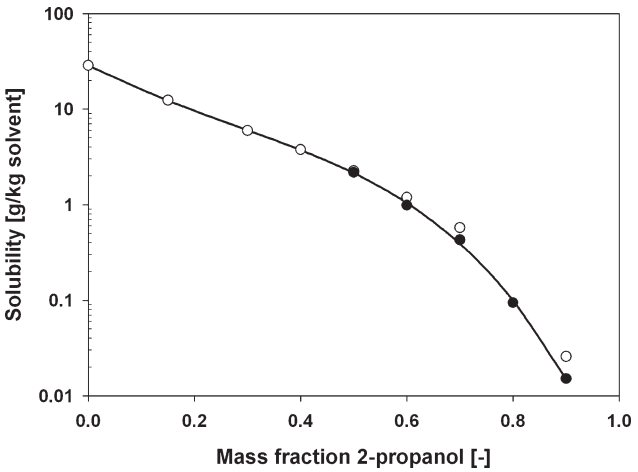

Figure 2. Solubility of L-asparagine monohydrate at 25°C in water–isopropanol solutions.

The filled circles represent the measurements carried out in this study, the open circles represent the data from the literature,[16] and the solid line represents the interpolation given by Eq. 2.

Table 2. Experimental Conditions of the Precipitation Experiments

Run	w (g/g)	S	t_{res} (s)	J (m^3/s)	d_{10} (μm)
1	0.52	3.7	10.5	$(8.6 \pm 4.4) \times 10^8$	1.6 ± 0.11
2	0.54	4.2	6.2	1.5×10^9	1.1
3	0.56	4.6	6.0	2.7×10^9	1.3
4	0.60	5.7	6.1	4.9×10^9	1.2
5	0.67	9.1	3.6	2.9×10^{10}	1.2
6	0.67	9.1	7.0	1.9×10^{10}	2.6
7	0.67	9.1	11.9	2.3×10^{10}	5.0
8	0.67	9.1	19.1	2.6×10^{10}	7.7
9	0.75	18	1.9	6.6×10^{10}	1.1
10	0.75	18	3.4	$(7.4 \pm 0.2) \times 10^{10}$	2.3 ± 0.16
11	0.75	18	7.9	4.8×10^{10}	4.4
12	0.75	18	14.0	6.9×10^{10}	7.8
13	0.85	52	2.0	8.3×10^{10}	1.5
14	0.85	52	3.9	6.3×10^{10}	3.2
15	0.85	52	8.9	7.9×10^{10}	6.6
16	0.85	52	18.7	7.2×10^{10}	9.0
17	0.89	81	2.2	$(2.5 \pm 0.3) \times 10^{11}$	2.0 ± 0.08
18	0.89	81	4.1	$(2.3 \pm 0.2) \times 10^{11}$	2.6 ± 0.19
19	0.89	81	9.8	2.4×10^{11}	7.0
20	0.89	81	15.9	2.2×10^{11}	7.9
21	0.95	169	2.7	2.1×10^{11}	1.5
22	0.95	169	5.2	2.4×10^{11}	3.5
23	0.95	169	11.9	2.2×10^{11}	5.2

Runs 1, 10, 17, and 18 were carried out three times and the standard deviation is given for the measured nucleation rate J and the particle size d_{10}; all other runs were carried out once.

$$J = \frac{dN}{dt}. \tag{3}$$

Based on the inspection of many microscope pictures at different supersaturations and residence times, significant agglomeration and breakage could not be observed in the early stages of the precipitation processes, i.e., in the first 20 s.

In each experiment, the solution at the outlet of the mixer was quenched after a predefined residence time t_{res} using a saturated solution and applying a quench ratio q of about 40. The exact quench ratio was determined by weighing the saturated solution before and after quenching. The residence time t_{res} can be varied using outlet pipes of different lengths.

The quenched solution was placed directly into the Coulter Multisizer. The constant volume mode, which measures the number of particles N in a sampling volume V_s (always 2 ml in our measurements), was used. The nucleation rate can be calculated using the following equation:

$$J = \frac{N}{t_{res}} \frac{q+1}{V_s}. \tag{4}$$

The nucleation rate given by Eq. 4 is an average nucleation rate, i.e., it is averaged over a distribution of mixing times, not an instantaneous one. However, if mixing is much faster than nucleation, as it is the case here (see time scale analysis section below), the effect of averaging is neglectable. Furthermore, it is assumed that the supersaturation remains constant before quenching.

The measured nucleation rates are given in Table 2. It must be noted that only particles above a size of 1 μm could be measured and that some error was introduced thereby. Therefore, the nucleation rate was measured at the same supersaturation but different residence times. The comparison of these nucleation rates shows a reasonably good agreement, whereas the standard deviations are $\sigma = 18\%$ for $S = 9.1$ (runs 5–8), $\sigma = 21\%$ for $S = 18$ (runs 9–11), $\sigma = 19\%$ for $S = 52$ (runs 13 and 14), and $\sigma = 6\%$ for $S = 81$ (runs 17 and 18), as calculated from the experimental data given in Table 2. The error introduced by the cut-off seems to be within the experimental error, i.e., the standard deviation of repeated experiments at identical conditions, which is in the range of 3–51% as given in Table 2 for $S = 3.7$ (run 1), $S = 18$ (run 10), and $S = 81$ (runs 17 and 18). Compared with other kinetics measurements, e.g., growth rates, the repeatability of the nucleation experiments is relatively poor, i.e., the average standard deviation of the measured nucleation rate is about 19%, and is in the same order of magnitude as for other substances.[17] The relatively poor repeatability might be attributed to different amounts of microscopic dust, which is very difficult to control and might promote heterogeneous nucleation. In each experiment, the actual supersaturation was calculated through an overall mass balance. If the supersaturation did not change by more than 5% across the mixer, these experiments were used for the determination of the kinetics. The other experimental data, i.e., runs 12, 15, 16, 19, 20, 22, and 23, were discarded.

According to the classical nucleation theory, nucleation kinetics can be described using the following expression[18]:

$$J = k_{J1} S \exp\left(-k_{J2} \frac{\ln^3 \frac{c_c}{c^*}}{\ln^2 S}\right), \tag{5}$$

where k_{J1} and k_{J2} are empirical parameters, c_c is given by ρ_c/M and c^* is the solubility in mol/m^3. The crystal density of L-asparagine ρ_c equals 1568 g/L, and the molecular mass M equals 150.14 g/mol.

The experimental nucleation rates divided by the supersaturation are plotted as a function of $\ln^3(c_c/c^*)/\ln^2 S$ in Figure 3. The empirical parameters in Eq. 5 can be determined by linear least-squares regression of the experimental data and are found to be:

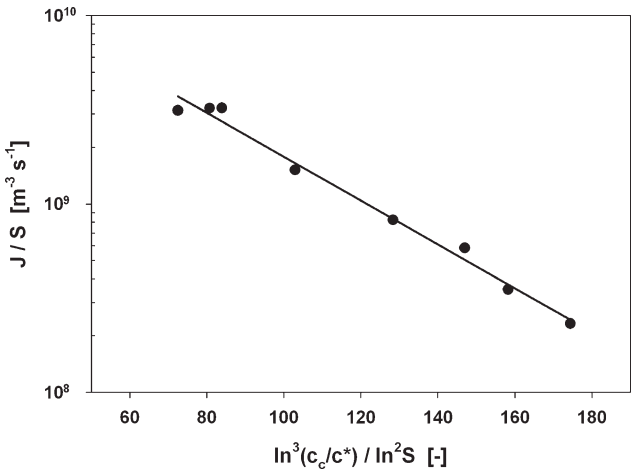

Figure 3. Nucleation rate of L-asparagine monohydrate divided by the supersaturation at 25°C.

Circles: experimental data; solid line: regression line.

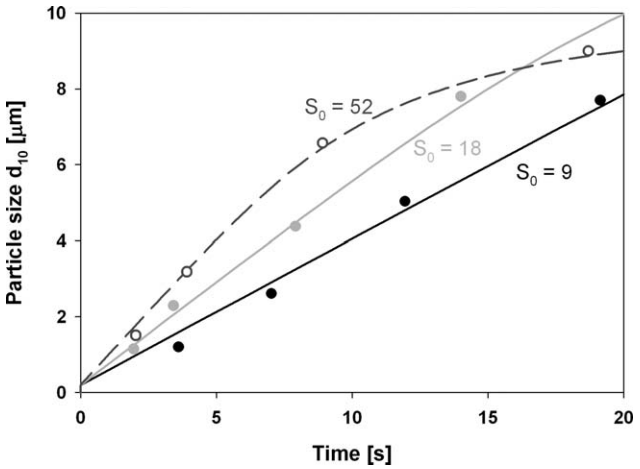

Figure 4. Average particle size d_{10} as a function of residence time and for different initial supersaturations.

Symbols: experimental data; lines: simulation results.

$$k_{J1} = 2.6 \times 10^{10} (\mathrm{m}^3/\mathrm{s}) \tag{6}$$

$$k_{J2} = 2.7 \times 10^{-2}. \tag{7}$$

The regression line has a regression coefficient of $R^2 = 0.99$ and is also plotted in Figure 3.

The estimated value k_{J2} can be used to calculate the experimental interfacial energy γ_{exp} as described elsewhere.[17,19] The values of γ_{exp} range from 11 to 19 mJ/m^2 for an antisolvent concentration from 50 to 90 wt %. These values can be compared with theoretical values for homogeneous nucleation.[18] The theoretical value of the interfacial energy is about four times larger than γ_{exp}. Moreover, the estimated value for k_{J1} is about 22 orders of magnitude lower than the predicted theoretical values of the kinetic parameter for homogenous nucleation.[19] This analysis indicates a heterogeneous nucleation mechanism for L-asparagine. The same observation has already been made for L-glutamic acid precipitation[17] and for several other organic compounds.[19]

Growth Kinetics. The growth kinetics of L-asparagine monohydrate were determined using the same set of experimental data as for the nucleation kinetics, i.e., runs 1–11, 13, 14, 17, and 18 in Table 2. The other runs were discarded because the initial supersaturation decreased by more than 5% across the mixer. Assuming agglomeration and breakage are negligible, the growth rate G can be calculated from the change of the crystal size over time:

$$G = \left.\frac{dL}{dt}\right|_{n=\mathrm{const}}. \tag{8}$$

The ith moment μ_i of the PSD is defined as

$$\mu_i = \int_0^\infty L^i n \, dL. \tag{9}$$

Assuming agglomeration and breakage can be neglected, the time derivative of the moments can be calculated as

$$\frac{d\mu_0}{dt} = J, \tag{10}$$

$$\frac{d\mu_i}{dt} = iG\mu_{i-1}, \quad i = 1, 2, \ldots. \tag{11}$$

At constant supersaturation, Eqs. 10 and 11 yield the following expressions for the moments of the PSD[20]:

$$\mu_0 = Jt \tag{12}$$

$$\mu_i = \frac{JG^i}{i+1} t^{i+1}. \tag{13}$$

Thus, the change of the average crystal size d_{10}, which is defined as the first moment divided by the zeroth moment of the PSD, can be calculated as

$$\frac{d(d_{10})}{dt} = \frac{d(\mu_1/\mu_0)}{dt} = \frac{d(Gt/2)}{dt} = \frac{G}{2}. \tag{14}$$

At each level of supersaturation, the PSD was measured at different residence times; a plot of the experimental average crystal size d_{10} over time, similar to those given in Figure 4, was used to calculate the average growth rate of the crystals. According to Eq. 14, the growth rate is equal to twice the slope of a straight line fitted through these data points using linear least-squares regression. The experimental growth rate as a function of the supersaturation is shown in Figure 5.

The following empirical expression for the growth kinetics was used to fit the experimental data, and by applying linear least-squares regression, the following parameters were estimated:

$$G = 3.82 \times 10^{-8} c^* (S-1)^{1.74}, \tag{15}$$

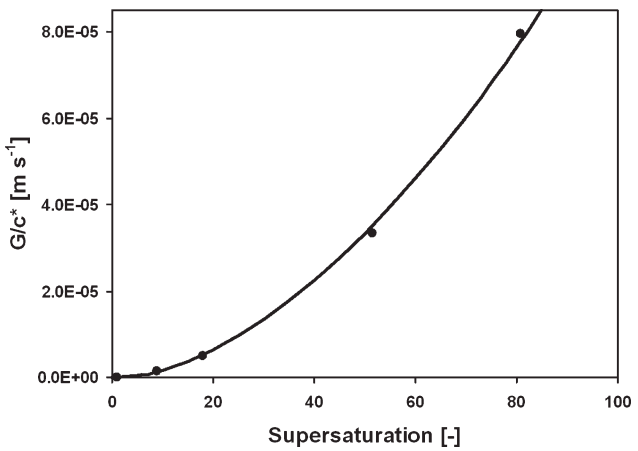

Figure 5. Growth rate G of L-asparagine monohydrate at 25°C normalized by the corresponding solubility c^*.

Circles: experimental data; solid line: fit of the experimental data described by Eq. 15.

where G is given in m/s and c^* in g/kg. The regression coefficient R^2 is 0.998. The value of 1.74 for the exponent in Eq. 15 is very reasonable as typical values are in the range of 1–2.[21] The estimated growth rate (Eq. 15) is plotted in Figure 5 as well.

Comparison with Literature Data. The nucleation and growth kinetics of L-asparagine were measured previously by Kirwan and Mahajan.[12] They used a similar approach for the determination of the kinetics. Induction times, nucleation, and growth kinetics were measured at a constant solvent composition of 50 vol % of 2-propanol and by using a grid mixer. As only equal volume flow rates could be realized in their setup, the maximum achievable supersaturation was about $S_0 = 4$. However, even at these low supersaturations, induction times as low as 1 s were measured. We could not reproduce these data in our laboratory; our induction times were about two orders of magnitude longer.

At a supersaturation of four, the nucleation kinetics found in the literature are about 15 times larger than the kinetics measured here. Accordingly, the interfacial energies are also quite different: 6.1 mJ/m^2 for the literature data as opposed to 10.3 mJ/m^2 for our kinetics. Comparison of the growth rates also shows significant differences, although the growth rates are in the same order of magnitude. At a supersaturation of four, the literature value is about four times larger than our data.

The differences between our results and the data from the literature cannot be explained convincingly. We can only make conjectures about the reason of the discrepancy; either the impurity profiles of the two sets of experiments were so different as to have a major influence on the kinetics of crystallization, or nucleation was in one of the two cases heavily controlled by reactor parts so as to make the comparison between the two independent measurements impossible. In addition, we would like to point to some differences between the two experimental procedures. In the procedure described in the literature, the flow is delivered using syringe pumps. Thus, the maximum experimental time is limited and conditions might not be stationary. Moreover, to achieve residence times longer than 360 ms the sample was held in the aging hose before quenching.[22] In our experiments, samples were taken at stationary conditions, i.e., after the flow rates had become constant, which was validated by measuring the flow rates of both inlet streams.

Precipitation Experiments and Modeling. The precipitation of L-asparagine monohydrate in the Y-mixer is modeled assuming plug flow through the mixer and using the population balance framework. The evolution of the PSD as a function of the position in the mixer is given by the following PBE model[23]:

$$u\frac{\partial n}{\partial z} + G\frac{\partial n}{\partial L} = 0, \tag{16}$$

where n is the number density of particles, u is the velocity, z is the position in the mixer, and G is the size-independent growth rate. The concentration c of the solute can be obtained by the material balance and is given by the following equation:

$$u\frac{dc}{dz} = -3k_v\rho_c G\int_{L_0}^{\infty} n L^2\, dL, \tag{17}$$

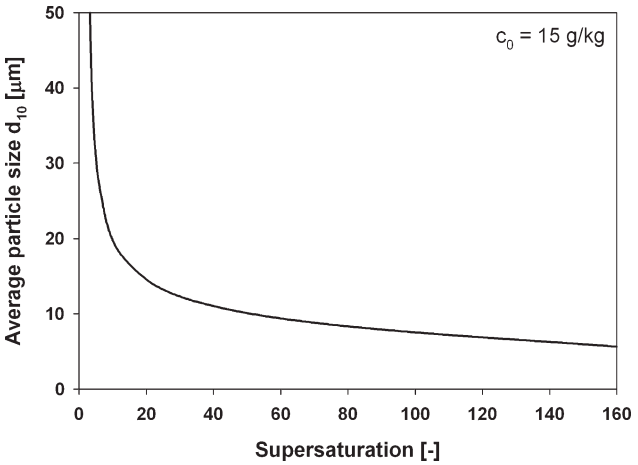

Figure 6. Simulated final average particle size d_{10} as a function of the initial supersaturation.

The initial concentration of L-asparagine in the inlet stream is always 15 g/kg.

with k_v being the volume shape factor. In this work, we have used a value of $k_v = \pi/6$. The following initial and boundary conditions apply for the PBE and the material balance:

$$n(L_0, z) = \frac{J}{G} \tag{18}$$

$$n(L, 0) = 0 \tag{19}$$

$$c(0) = c_0, \tag{20}$$

where c_0 is the initial solute concentration. The PBE is solved using the method developed by Kumar and Ramkrishna[24] as described elsewhere.[25] The spatial evolution of the PSD can be converted to a temporal one using the following equation:

$$t = \frac{z}{u}, \tag{21}$$

where t is the time.

The plug flow model is a reasonable simplification only if the time scales for mixing are much smaller than those for precipitation, i.e., if the course of the precipitation process is not affected by the mixing conditions. In the following sections, the model results for the precipitation experiments in the Y-mixer (see sections on nucleation and growth kinetics) are presented. The model uses the nucleation and growth kinetics given by Eqs. 5 and 15, respectively, together with the solubility given by Eq. 2.

The evolution of the average particle size d_{10} is shown in Figure 4 for different initial supersaturations, i.e., $S = 9$ (runs 5–8), $S = 18$ (runs 9–12), and $S = 52$ (runs 13–16). The initial concentration in the solute stream was constant at 15 g/kg, and the supersaturation was varied by changing the flow rate ratio between the solute and the antisolvent stream. The agreement between model and experiment is good in a rather broad supersaturation range. It can be observed that at fixed (residence) time the particle size increases with increasing supersaturation. However, the final particle size decreases with increasing initial supersaturation as shown in Figure 6.

The particle size can be controlled either by quenching after a certain residence time or by adjusting the initial supersaturation. The first method has the disadvantage that large amounts of solvent are necessary, which might make this option unattractive for industrial applications. In turn, the second method does not allow for producing any desired particle size. In fact, the final particle size depends on the intrinsic ratio of nucleation and growth and the dependence of this ratio on supersaturation. It is plotted as a function of the supersaturation in Figure 6; in the supersaturation range studied here the particle size can be varied between 5 and 50 μm. Moreover, secondary effects such as agglomeration and breakage are sometimes important, e.g., agglomeration often becomes the dominant mechanism for very small particles.

Simultaneous Kinetics Estimation. Most particle size measurement techniques, e.g., the widely used laser diffraction methods, measure only the normalized PSD, and the number concentration cannot be determined. Therefore, we want to check if the kinetics can also be determined based on the evolution of the average particle size along the mixer. In total, experimental data at five different initial supersaturation levels, namely 9, 18, 52, 81, and 169, and in a range of residence times between 1 and 20 s were used for the parameter estimation (runs 5–23 in Table 2). Some of the experimental data that was used for the kinetics estimation is shown in Figure 4. The parameters in the kinetic expressions for nucleation and growth are estimated simultaneously on the basis of these precipitation experiments using a nonlinear optimization algorithm that minimizes the sum of square residuals, SSR, between the experimental and simulated values of the average particle size:

$$\mathrm{SSR} = \sum_{i=1}^{N_\mathrm{e}} \sum_{j=1}^{N_{\mathrm{d},i}} \left(d_{10,i,j}^{\mathrm{exp}} - d_{10,i,j}^{\mathrm{sim}} \right)^2, \tag{22}$$

where N_e is the number of experiments at different initial supersaturations, $N_{\mathrm{d},i}$ is the number of data points at different residence times per experiment i, and d_{10}^{exp} and d_{10}^{sim} are the experimental and simulated average particle sizes, respectively. The PBE model given by Eqs. 16–20 was applied for the simulations. The optimization problem was solved using the *lsqnonlin* algorithm of the MATLAB optimization toolbox. Changing the initial values of the estimated parameters in the optimization procedure over several orders of magnitude always produced the same results, thus indicating the existence of a global optimum.

Approximate confidence intervals of the model parameter b can be determined by calculating the sensitivity matrix, i.e., the derivative of the model predictions with respect to the model parameters, based on a linearized model in the vicinity of the estimated values.[26] The sensitivity matrix can be used to calculate the approximate covariance matrix of the estimated parameters. The standard error s_k of the kth model parameter is given by the square root of the kth diagonal element of this covariance matrix.[26] The confidence intervals of the kth parameter are given by

$$b_k \pm t_{\alpha,\nu} s_k, \tag{23}$$

where $t_{\alpha,\nu}$ is the value of the t-distribution for confidence interval α in the case of ν degrees of freedom. We have used $\alpha = 0.05$ leading to a 95% confidence interval.[26]

As a result of the parameter estimation we have obtained the following kinetics:

$$J = (6.3 \pm 1.6) \times 10^{10} S \exp\left((-3.9 \pm 0.5) \times 10^{-2} \frac{\ln^3 \frac{c_\mathrm{e}}{c^*}}{\ln^2 S} \right) \tag{24}$$

$$G = (3.9 \pm 0.3) \times 10^{-8} c^* (S-1)^{(1.73 \pm 0.02)}. \tag{25}$$

The approximate correlation matrix can be obtained using the covariance matrix of the estimated parameters as described elsewhere.[26] The off-diagonal elements of the correlation matrix relating the nucleation and the growth rate parameters are in the range between 0.11 and 0.37. Thus, it can be concluded that the nucleation and growth kinetics are only slightly correlated.[26] A comparison of the growth rates given by Eqs. 15 and 25 shows a very good agreement between the two different techniques for the determination of growth rates. In fact, the independently measured growth rate Eq. 15 is within the (rather narrow) confidence interval of the simultaneously estimated growth rate Eq. 25. However, the two nucleation rates given by Eqs. 5–7 and 24 differ significantly. It must be noted that the confidence intervals of the nucleation rate parameters are much larger than those for the growth rate, i.e. the estimation of the nucleation rate is less accurate. A comparison of the simulated time evolution of d_{10} shows that the curves for the model using the independently measured kinetics and for the model using the simultaneously estimated kinetics coincide for all precipitation experiments.

It can be concluded that the method for the simultaneous estimation of nucleation and growth kinetics based on the measurements of the average particle size yields similar results, when compared with the independent determination. However, this might not be true in all cases, and the correlation matrix should always be calculated to check whether or not the kinetics are highly correlated.

Time scale analysis

The mixer setup is used to determine true kinetics, i.e., kinetics that are not affected by mixing. Obviously, the precipitation time scales are not known before measuring the kinetics. Therefore, a time scale analysis should be conducted by hindsight to validate if there were actually no mixing limitations during the experiments used for the determination of the kinetics. Moreover, the plug flow model used earlier is also valid only if the time scales for mixing are much smaller than those for precipitation.

Average mixing times in the Y-mixer have been determined previously[6,15] and are used here as characteristic time scale for mixing. For the flow rate, flow rate ratio, and viscosity ratio applied here, mixing time scales are always below 20 ms.

The characteristic time scale for nucleation τ_N is the induction time, which can be estimated as follows[27]:

$$\tau_N = \left(\frac{4\,\alpha_v}{k_v J G^3}\right)^{1/4}, \tag{26}$$

with α_v being the detectable volume fraction. A value of 0.1% of the maximum solid concentration is chosen arbitrarily for α_v:

$$\alpha_v = 0.001(c_0 - c^*), \tag{27}$$

where c_0 and c^* are the initial and equilibrium concentrations, respectively, both given in m^3/m^3.

The characteristic time scale for growth τ_G describes the rate of concentration decrease resulting from crystal growth and can be calculated as follows[28]:

$$\tau_G = c/(\rho_c a_c G), \tag{28}$$

with a_c being the specific surface of the crystals in the reactor. A typical value for L-asparagine and the condition studied here is $a_c = 100\ m^2/m^3$.

The characteristic time scales as a function of the supersaturation are shown in Figure 7. It can be readily observed that the precipitation time scales are at least one order of magnitude larger than the mixing time scale. Thus, the precipitation process is not affected by the mixing conditions. It should also be noted that mixing time scales in static micromixers can be as low as 0.1 ms,[6,15], i.e., three orders of magnitude lower than the precipitation time scales.

To validate the aforementioned analysis, the particle size of L-asparagine monohydrate crystals was measured at different flow rates and fixed supersaturation and residence time. The initial concentration of L-asparagine monohydrate was 15 g/kg in the solute stream, the flow rate ratio was 1:8 (solute:antisolvent), and the corresponding initial supersaturation was 88. The residence time was 11 s and was adjusted to the flow rate by changing the length of the outlet tube. The experimental average particle size d_{10} is plotted in Figure 8 as a function of the flow rate of the larger stream. It can be observed that the particle size is independent of the flow rate, thus supporting the result of the time scale analysis, namely that mixing is much faster than precipitation.

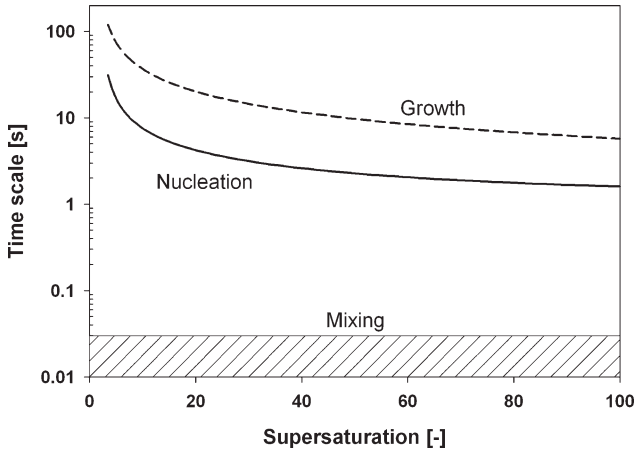

Figure 7. Characteristic nucleation, growth, and mixing time scales as a function of supersaturation.

The initial concentration of L-asparagine in the inlet stream is always 15 g/kg.

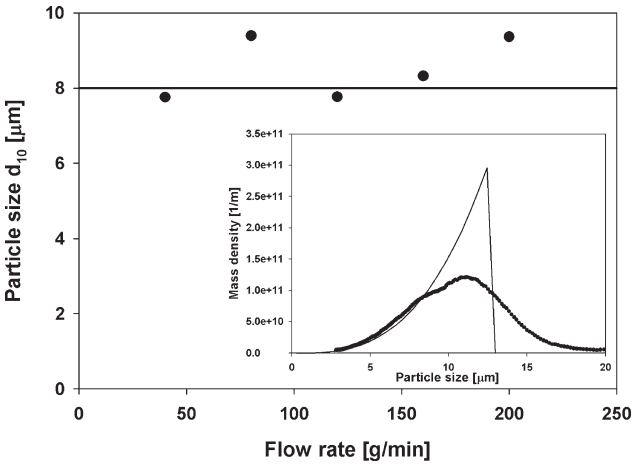

Figure 8. Measured average particle size d_{10} for different flow rates (symbols) and corresponding simulation result (line).

The residence time is 11 s, and the initial supersaturation is $S_0 = 88$ in each experiment. The inset shows the PSD at a flow rate of 200 g/min (symbols: experiment; line: simulation).

The corresponding simulation results are plotted in Figure 8 as well, and a good agreement with the experimental data can be observed. In this case, the model is used in a fully predictive manner. It must be noted that the plug flow model does not account for mixing effects. Thus, at fixed residence time the final particle size does not depend on the flow rate.

A comparison of the simulated and the measured PSD at a flow rate of 200 g/min is shown in the inset of Figure 8. It can be observed that the experimental PSD is slightly broader and shifted toward larger particle sizes, when compared with the simulated PSD. The broadening of the PSD might be attributed to agglomeration, growth rate dispersion, hydrodynamic backmixing, or to the sampling procedure.[14] However, studying the effect of these parameters on the PSD was beyond the scope of this work.

Conclusions

In this work, a technique for the production of small micron-sized crystalline particles was presented. It is based on a precipitation process carried out at high supersaturation levels and in a static mixer to avoid transport limitations. Nucleation and growth kinetics of L-asparagine monohydrate precipitated by antisolvent addition were determined for a wide range of supersaturations, i.e. from about 4 to 170. Two different methods for the kinetics estimation were compared. In the first method, nucleation and growth kinetics were measured independently, whereas the nucleation rate was calculated from the change of particle concentration over time, and the growth rate was calculated based on the change of the particle size over time. In the second method, nucleation and growth kinetics were estimated simultaneously based on the time evolution of the experimental particle size by a combination with a population balance model

and an integral parameter estimation technique. It was found that both methods yield similar kinetics; however, it should always be checked if the kinetics parameters are highly correlated. The precipitation of L-asparagine monohydrate in the Y-mixer was modeled assuming plug flow through the mixer and using the population balance framework. The model was in good agreement with the experimental data and was used to design a continuous precipitation process. A time scale analysis showed that mixing is much faster than precipitation and therefore the two processes could be decoupled.

Notation

Roman letters

a_c = specific surface area, m^2/m^3
c = concentration, mol/m^3
c^* = solubility, g/kg of solvent
d_{ij} = average particle size: ith divided by jth moment of PSD, m
G = growth rate, m/s
J = nucleation rate, m^3/s
k = empirical parameter, dimensionless
k_v = volume shape factor, dimensionless
L = particle size, m
n = number density, m^{-4}
N = number of particles, m^{-3}
M = molecular mass, g/mol
q = quench ratio, g/g
R^2 = regression coefficient, dimensionless
S = supersaturation, dimensionless
t = time, s
t_i = induction time, s
u = velocity, m/s
V_s = sampling volume, m^3
w = antisolvent concentration, g/g
z = position, m

Greek letters

α_v = detectable volume fraction, m^3/m^3
γ = interfacial energy, J/m^2
μ_i = ith moment of the PSD, m^i/m^3
ρ_c = crystal density, kg/m^3
τ = time scale, s

Literature Cited

1. Stahl M, Rasmuson AC. Towards predictive simulation of single feed semibatch reaction crystallization. *Chem Eng Sci*. 2009;64:1559–1576.
2. Woo XY, Tan RBH, Chow PS, Braatz RD. Simulation of mixing effects in antisolvent crystallization using a coupled CFD–PDF–PBE approach. *Cryst Growth Des*. 2006;6:1291–1303.
3. Vicum L, Mazzotti M. Multi-scale modeling of a mixing-precipitation process in a semibatch stirred tank. *Chem Eng Sci*. 2007;62:3513–3527.
4. Baldyga J, Makowski L, Orciuch W. Interaction between mixing, chemical reactions, and precipitation. *Ind Eng Chem Res*. 2005;44:5342–5352.
5. Baldyga J, Makowski L, Orciuch W. Double-feed semibatch precipitation—effects of mixing. *Chem Eng Res Des*. 2007;85:745–752.
6. Lindenberg C, Schöll J, Vicum L, Brozio J, Mazzotti M. Experimental characterization and multi-scale modeling of mixing in static mixers. *Chem Eng Sci*. 2008;63:4135–4149.
7. Schwarzer HC, Schwertfirm F, Manhart M, Schmid HJ, Peukert W. Predictive simulation of nanoparticle precipitation based on the population balance equation. *Chem Eng Sci*. 2006;61:167–181.
8. Woo XY, Tan RBH, Braatz RD. Modeling and computational fluid dynamics–population balance equation–micromixing simulation of impinging jet crystallizers. *Cryst Growth Des*. 2009;9:156–164.
9. Mahajan AJ, Kirwan DJ. Micromixing effects in a two-impinging-jets precipitator. *AIChE J*. 1996;42:1801–1814.
10. Liu Y, Cheng CY, Liu Y, Prud'homme RK, Fox RO. Mixing in a multi-inlet vortex mixer (MIVM) for flash nano-precipitation. *Chem Eng Sci*. 2008;63:2829–2842.
11. Mahajan AJ, Kirwan DJ. Rapid precipitation of biochemicals. *J Phys D: Appl Phys*. 1993;26:B176–B180.
12. Mahajan AJ, Kirwan DJ. Nucleation and growth-kinetics of biochemicals measured at high supersaturations. *J Cryst Growth*. 1994;144:281–290.
13. Blandin AF, Mangin D, Nallet V, Klein JP, Bossoutrot JM. Kinetics identification of salicylic acid precipitation through experiments in a batch stirred vessel and a T-mixer. *Chem Eng J*. 2001;81:91–100.
14. Stahl M, Alund BL, Rasmuson AC. Reaction crystallization kinetics of benzoic acid. *AIChE J*. 2001;47:1544–1560.
15. Lindenberg C, Mazzotti M. Experimental characterization and multi-scale modeling of mixing in static mixers. Part 2. Effect of viscosity and scale-up. *Chem Eng Sci*. 2009;64:4286–4294.
16. Orella CJ, Kirwan DJ. Correlation of amino-acid solubilities in aqueous aliphatic alcohol-solutions. *Ind Eng Chem Res*. 1991;30:1040–1045.
17. Lindenberg C, Mazzotti M. Effect of temperature on the nucleation kinetics of α L-glutamic acid. *J Cryst Growth*. 2009;311:1178–1184.
18. Kashchiev D, van Rosmalen GM. Review: nucleation in solutions revisited. *Cryst Res Technol*. 2003;38:555–574.
19. Roelands CPM, ter Horst JH, Kramer HJM, Jansens PJ. Analysis of nucleation rate measurements in precipitation processes. *Cryst Growth Des*. 2006;6:1380–1392.
20. Vollmer U, Raisch J. Control of batch cooling crystallization processes based on orbital flatness. *Int J Control*. 2003;76:1635–1643.
21. Mersmann A.*Crystallization Technology Handbook*, 2nd ed. New York: Marcel Dekker Inc., 2001.
22. Mahajan AJ. Rapid precipitation of biochemicals: kinetics and micromixing, *PhD Thesis*, University of Virginia, 1993.
23. Randolph A, Larson MA. *Theory of Particulate Processes*, 2nd ed. San Diego, CA: Academic Press, 1988.
24. Kumar S, Ramkrishna D. On the solution of population balance equations by discretization. III. Nucleation, growth and aggregation of particles. *Chem Eng Sci*. 1997;52:4659–4679.
25. Lindenberg C, Schöll J, Vicum L, Brozio J, Mazzotti M. L-Glutamic acid precipitation: agglomeration effects. *Cryst Growth Des*. 2008;8:224–237.
26. Beck JV, Arnold KJ. *Parameter Estimation in Engineering and Science*, 1st ed. New York: Wiley, 1977.
27. Kashchiev D, Verdoes D, Vanrosmalen GM. Induction time and metastability limit in new phase formation. *J Cryst Growth*. 1991;110:373–380.
28. Baldyga J, Bourne JR. *Turbulent Mixing and Chemical Reactions*, 1st ed. Chichester: Wiley, 1999.

Manuscript received Jun. 22, 2009, and revision received May 5, 2010.